Ab Initio Investigation of the Electronic and Geometric Structure of Magnesium Diboride, MgB_2

Demeter Tzeli and Aristides Mavridis*

Laboratory of Physical Chemistry, Department of Chemistry, National and Kapodistrian University of Athens, P.O. Box 64 004, 157 10 Zografou, Athens, Greece

Received: May 25, 2005

Employing multireference variational (MRCI) and coupled cluster (CC) methods combined with quadruple-ζ quality correlation-consistent basis set, we have studied 36 states of the magnesium diboride (MgB_2) molecule as well as 17 states of the experimentally unknown diatomic MgB. For all states of MgB_2, we report geometries, atomization energies, and dipole moments, while for the first 5 states, potential energy profiles have been also constructed. The ground state is formally of $^1A_1$ V-shaped symmetry with an atomization energy of 108.1(109) kcal/mol at the MRCI(MRCI + Davidson correction) level. The first excited state ($^3B_1$) is less than 1 kcal/mol above the $\tilde{X}^1A_1$ state, with the next state of linear Mg−B−B geometry ($\tilde{b}^3\Sigma^-$) located 10 kcal/mol higher. In all states, bent or linear, the bonding is complicated and unconventional because of the extraordinary bonding agility of the boron atom(s).

1. Introduction

In 2001, Jun Akimitsu's group[1] discovered that the simple compound magnesium diboride (MgB_2) becomes superconducting at the transition temperature $T_c = 39$ K, almost twice as large compared to the highest T_c among the intermetallics, namely, that of Nb_3Ge ($T_c = 23$ K).[2] Given the chemical simplicity of MgB_2 as well as its simple crystal structure,[1,3] the natural abundance of its constituent elements, and therefore the prospects for plausible applications, this was indeed a remarkable discovery. The enthusiastic response of the scientific community was testified to by a series of experimental[4] and theoretical[5] publications.

It is worthwhile to recall at this point that the elements Mg and B have played a fundamental role in the development of "pure and applied chemistry" as only the names of "Grignard reagent" (RMgX) and "boron hydrides" (B_xH_y) suggest.[6] And although MgB_2 has been well-characterized since the early fifties,[3] until now nobody suspected its unusual properties. Experimenters using different techniques have already established a variety of sometimes "conflicting" properties, for example, the existence of two superconducting gaps in MgB_2 which had not been seen before in any material.[2]

Obviously, all the above characteristics of MgB_2 refer to the solid state. On the other hand, there are three very recent theoretical ab initio works on the isolated noninteracting MgB_2 molecule. The first one by Ercoç in 2003 was conducted at a very low level of theory;[7] in 2004, Yang et al.[8] calculated 9 states (6 linear and 3 bent) around equilibrium using the QCISD/6-311G* and CCSD(T)/cc-pVTZ methods predicting different ground states, $^3B_1$ and $^1A_1$, respectively. However, on the basis of their CCSD(T) results, they concluded that the ground state is of $^1A_1$ symmetry with the $^3B_1$ state 412 cm^{-1} higher. A few months later, Lee and Wright[9] published the investigation of 21 states of MgB_2 around equilibrium using a variety of methods, MP2, DFT(B3LYP), QCISD, UCCSD(T), and RCCSD(T), employing a 6-311+G (3df) basis set. Not all 21 states have been calculated at all levels of theory, only at MP2. Ten of the 21 states have been calculated at the DFT level with conflicting results as compared to the MP2 values. At the QCISD and UCCSD(T) levels, they calculated 3 states, again with conflicting results between these 2 methods. Now, at the RCCSD(T) level and using a correlation-consistent aug-cc-pVQZ basis, they obtained the first 4 states around equilibrium. Then, they recalculated these 4 states by including core functions on B and Mg, but at the geometry of the previous level. Finally, they also performed MRCI/aug-cc-pVQZ//RCCSD(T)/aug-cc-pVQZ, i.e., single-point calculations, for these 4 lowest states. At this level of theory, Lee and Wright[9] concluded as well that the ground state is of $^1A_1$ symmetry with the $\tilde{a}^3B_1$ about 0.4 kcal/mol higher.[9]

Motivated by the remarkable properties of crystalline MgB_2 and the somehow conflicting theoretical results reported so far,[8,9] we herein report ab initio calculations using multireference and coupled-cluster methods in conjunction with quantitative correlation-consistent basis sets. In both methods, the symmetry of the ground state seems to be $^1A_1$ (but, see below).

We have examined a total of 36 states, reporting energetics, dipole moments, geometric and spectroscopic parameters, and Mulliken densities. In addition, for the first 5 states, we have constructed potential energy profiles of the corresponding potential surfaces, while some emphasis is given in explaining the bonding with the help of simple valence-bond-Lewis (vbL) diagrams.

In section 2, we define the computational procedure followed; in section 3, we present our results on the diatomics MgB and B_2 and on the triatomic MgB_2, and in section 4, some final remarks and comments are presented.

2. Computational Procedure

For the Mg and B atoms, the correlation-consistent basis by Dunning[10] of quadruple cardinality, cc-pVQZ = 16s12p3d2f1g and 12s6p3d2f1g, respectively, were employed through all

* E-mail: mavridis@chem.uoa.gr.

10.1021/jp058172b CCC: $30.25
Published on Web 11/05/2005

calculations. Both sets were generally contracted to [6s5p3d2f1g/$_{\text{Mg}}$ 5s4p3d2f1g/$_{\text{B}}$], amounting to 169 spherical Gaussian functions for the MgB_2 system.

Our general approach is the complete active space self-consistent field (CASSCF) method, extended to the single and double replacements out of the zeroth-order CASSCF wave function (CASSCF + 1 + 2 = MRCI), to account for "dynamical" correlation. Our reference space is built by allotting the 8 (chemically) active electrons of MgB_2 ($3s^2$ on Mg and $2s^2 2p^1$ on each B atom) among 12 orbital functions (3s and 3p on Mg + 2s and 2p on B's). The ensuing CASSCF wave function expansions range from 12 776 ($^5B_2$; BMgB) to 28 376 ($^3B_2$; BMgB) configuration functions (CF), with MRCI spaces ranging from 111×10^6 (MgBB; $^1\Sigma^-$) to 202×10^6 (MgBB; $^3\Sigma^-$) CFs. By applying the internal contraction (icMRCI) approximation,[11] the number of CFs is reduced by more than an order of magnitude, thus making the calculations feasible. Size nonextensivity errors do not exceed 2 mh at the icMRCI level, reduced to about 0.5 mh by including the Davidson correction for quadruples (+Q).

For the four lowest states, $\tilde{X}^1A_1$ (BMgB), $^3B_1$ (BMgB), $^3\Sigma^-$ (MgBB), and $^5\Sigma^-$ (MgBB), the coupled-cluster single reference + singles + doubles + perturbative connected triples method [RCCSD(T)] as implemented in MOLPRO [12] was also used. Note that both SCF and CASSCF orbitals were used for the construction of the single reference function. For the $^1A_1$ state only, Møller−Plesset MP2 and MP4 calculations were also tried with the harmonic frequencies obtained at the MP2/cc-pVQZ level of theory.

Finally, concerning the diatomic molecules MgB and B_2, we have examined 17 and 5 states, respectively, at the ic-MRCI/cc-pVQZ level and within the spirit outlined above.

3. Results and Discussion

A. The Diatomics MgB and B_2. In the present work, two geometrical isomers of MgB_2 are examined, namely, B−Mg−B and Mg−B−B: Both can be thought of as products of the interaction channels MgB + B or Mg + B_2. Therefore, for a better understanding of MgB_2, the study of both diatomics MgB and B_2 is rather mandatory.

It is rather surprising that no experimental results are available for MgB. Theoretically, we are aware of only two publications on MgB by Boldyrev et al.[13] and by Machado and co-workers.[14] The former authors investigated the first four states $X^2\Pi$, $A^2\Sigma^+$, $^4\Pi$, and $^4\Sigma^-$ and a higher excited state of $^2\Pi$ symmetry around equilibrium, in a variety of single reference methods, namely, MP2(full)/6-311+G*, QCISD(T)/6-311+G(2df), and MP4/6-311+G*//MP2/6-311+G*. Machado et al.[14] examined the first two states of BeB, MgB, and CaB using a (truncated) MRCISD/6-311+G(3d1f).

On the contrary, B_2 is a well-explored molecule both experimentally[15] and theoretically.[16] Nevertheless, for reasons of uniformity and completeness, the five lowest states of the B_2 molecule are currently examined at the MRCI/cc-pVQZ level.

The MRCI energy splittings of Mg [^{1}P, ^{3}P($3s^1 3p^1$) ← ^{1}S($3s^2$)] and B atoms [^{4}P($2s^1 2p^2$) ← ^{2}P($2s^2 2p^1$)] are in excellent agreement with experiment (in parentheses[17]): 2.603 (2.714), 4.318 (4.346), and 3.591 (3.571) eV, respectively. These three excited states are actively involved in the calculated states of MgB, B_2, and MgB_2.

MgB. Table 1 lists the energetics, the usual spectroscopic parameters, and the dipole moments of 17 states of MgB, spanning an energy range of about 4.2 eV, correlating adiabatically to Mg(^{1}S) + B(^{2}P, ^{4}P), Mg(^{3}P) + B(^{2}P), and Mg(^{3}P) + B(^{4}P) ($16^6\Sigma^-$). Corresponding potential energy curves (PECs) are plotted in Figure 1. Table 2 presents leading CASSCF configurations and Mulliken atomic populations of the first four states of MgB ($X^2\Pi$, $A^2\Sigma^+$, $2^4\Sigma^-$, and $3^4\Pi$). The valence-bond-Lewis (vbL) bonding diagrams of these four states based on their CFs and population densities are shown below.

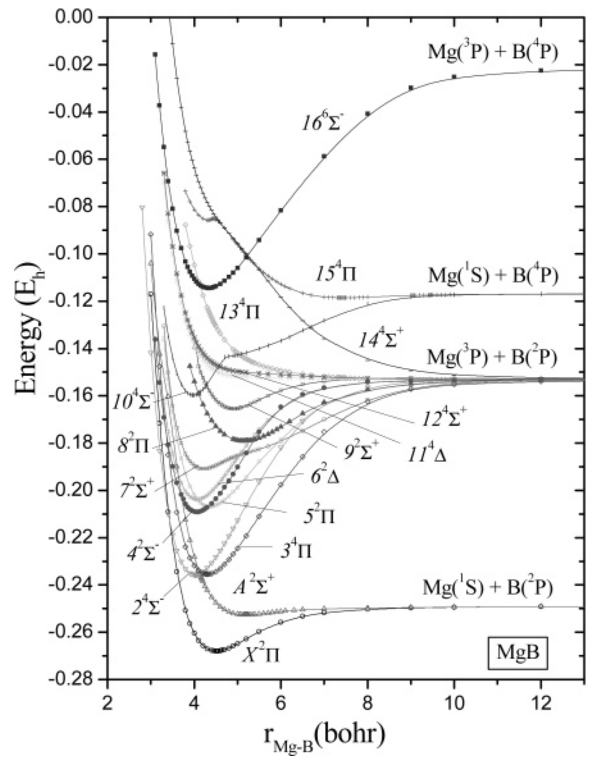

Figure 1. Potential energy curves of 17 states of the MgB molecule at the MRCI/cc-pVQZ level of theory. All energies have been shifted by +224 E_h.

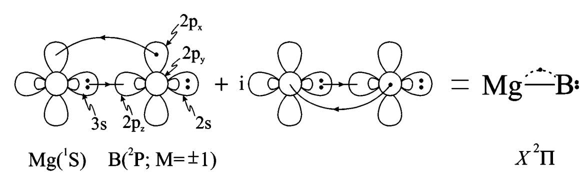

(1)

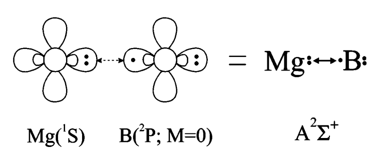

(2)

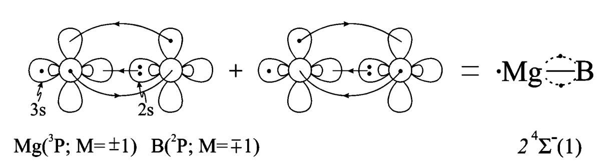

(3)

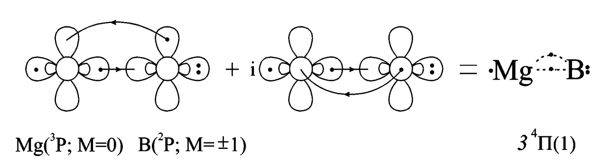

(4)

The ground state of MgB is of $^2\Pi$ symmetry with a binding energy and internuclear distance of D_e = 11.85 (12.7) kcal/mol and r_e = 2.3862 (2.383) Å, respectively, at the MRCI-

TABLE 1: Absolute Energies E (hartree), Bond Lengths r_e (Å), Binding Energies D_e (kcal/mol) with Respect to the Adiabatic Fragments, Harmonic Frequencies and Anharmonic Corrections ω_e, $\omega_e x_e$ (cm^{-1}), Rotational Vibrational Couplings α_e (cm^{-1}), Centrifugal Distortions $\bar{D}_e$(cm^{-1}), Mulliken Charges on B q_B, Dipole Moments μ (debye), and Energy Separations T_e (kcal/mol) of the MgB Molecule at CASSCF, MRCI,[a] and MRCI+Q[b]/cc-pVQZ Levels. Other Theoretical Results Are Also Included.

state	method	$-E$	r_e	D_e	ω_e	$\omega_e x_e$	α_e (10^{-3})	$\bar{D}_e$ (10^{-6})	$-q_B$	$\langle\mu\rangle/\mu_{FF}$[c]	T_e
$X^2\Pi$	CASSCF	224.211593	2.4423	2.69	310.9	12.4	10.6	2.18	0.24	1.86/1.86	0.0
	MRCI	224.267947	2.3862	11.85	365.9	6.14	6.80	1.80	0.31	2.38/2.39	0.0
	MRCI+Q	224.27062	2.383	12.7						/2.44	0.0
	MP2(full)/6-311+G*[d]	224.351223	2.473		269						0.0
	QCISD(T)/6-311+G(2df)[d]	224.25419	2.390	10.8							0.0
											0.0
$A^2\Sigma^+$	CASSCF	repulsive									
	MRCI	224.252702	2.7515	2.28	192.3	10.6	12.1	2.79	0.04	−0.42/−0.41	9.57
	MRCI+Q	224.25481	2.730	2.83						/−0.31	9.92
	MP2(full)/6-311+G*[d]	repulsive									
	QCISD(T)/6-311+G(2df)[d]	224.23962	2.775	1.7							9.1
$2^4\Sigma^-(1)$	CASSCF	224.183512	2.1605	47.97	525.5	3.20	4.44	1.59	0.35	3.37/3.37	17.6
	MRCI	224.235687	2.1259	51.98	554.9	3.54	4.54	1.57	0.39	3.85/3.84	20.2
	MRCI+Q	224.23792	2.126	52.2						/3.87	20.5
	MP2(full)/6-311+G*[d]	224.32603	2.117		568						15.8
	QCISD(T)/6-311+G(2df)[d,e]	224.22221									20.1
$3^4\Pi(1)$	CASSCF	224.182164	2.2703	45.33	446.7	1.66	6.20	1.62	0.40	2.04/2.04	18.5
	MRCI	224.235411	2.2769	51.61	474.8	0.01	2.52	1.41	0.37	1.98/1.92	20.4
	MRCI+Q	224.23820	2.276	52.3						/1.92	20.3
	MP2(full)/6-311+G*[d]	224.33561	2.263		510						9.8
	QCISD(T)/6-311+G(2df)[d,e]	224.22283									19.7
$4^2\Sigma^-(1)$	CASSCF	224.153555	2.1973	26.07	493.2	3.40	3.72	1.63	0.47	2.13/2.13	36.4
	MRCI	224.209085	2.1496	35.04	517.0	5.42	12.3	1.71	0.47	2.64/2.80	36.9
	MRCI+Q	224.21202	2.149	35.9						/2.81	37
$5^2\Pi(2)$	CASSCF[f]	224.14056	2.338	20.1	424.5	4.03	3.84	1.51	0.35	1.89/2.05	44.6
	MRCI	224.20685	2.305	33.7	458.1	4.39	4.98	1.42	0.37	2.12/2.03	38.3
	MRCI+Q	224.2116	2.308	35.6						/2.05	37
$6^2\Delta(1)$	CASSCF[f]	224.13460	2.203	17.9	460.6	5.80	4.80	1.84	0.23	2.02/2.59	48.3
	MRCI	224.20383	2.151	31.8	521.0	5.37	6.46	1.66	0.35	3.25/3.30	40.2
	MRCI+Q	224.2083	2.157	33.2						/3.35	39
$7^2\Sigma^+(2)$	CASSCF[f]	224.12767	2.264	13.4	379.3	11.0	9.29	2.31	0.20	1.75/1.93	52.7
	MRCI	224.19086	2.231	23.7	404.8	7.87	8.76	2.22	0.25	2.37/2.37	48.4
	MRCI+Q	224.1946	2.235	24.7						/2.35	48
$8^2\Pi(3)$	CASSCF[f]	224.11286	2.757	4.74	303.8	6.68	3.53	1.10	0.18	0.87/0.67	62.0
	MRCI	224.17914	2.724	16.4	280.8	0.98	1.86	1.38	0.04	−0.30/−0.34	55.7
	MRCI+Q	224.1841	2.712	18.1						/−0.50	54
$9^2\Sigma^+(3)$	CASSCF[f]	224.10555	3.023	−0.38					0.07	0.55/0.15	66.5
	MRCI	224.16548	2.596	7.77	357.8	8.87	4.40	1.14	0.15	0.46/0.43	64.3
	MRCI+Q	224.1703	2.548	9.5						/0.58	63
$10^4\Sigma^-(2)$	CASSCF[f]	224.09820	2.186	4.32	414.2	28.8	16.4	2.43	0.39	3.24/3.55	71.2
	MRCI	224.15975	2.104	26.9	618.1	6.10	3.15	1.35	0.39	3.83/3.86	67.9
	MRCI+Q	224.1636	2.104	29.0						/3.89	67
$11^4\Delta(1)$		repulsive									
$12^4\Sigma^+(1)$		repulsive									
$13^4\Pi(2)$	CASSCF	repulsive									
	MRCI	224.15321	5.000	0.22					0.00	−0.08/−0.11	72.0
	MRCI+Q	224.1555	4.799	0.26						/−0.14	72
$14^4\Sigma^+(2)$		repulsive									
$15^4\Pi(3)$	CASSCF	repulsive									
	MRCI	224.11855	3.945	1.04					0.02	0.08/0.07	93.7
	MRCI+Q	224.1196	3.881	1.29						/0.14	95
$16^6\Sigma^-(1)$	CASSCF	224.08667	2.303	49.8	437.3	2.44	3.88	1.57	0.49	3.00/3.00	78.4
	MRCI	224.11443	2.293	58.2	441.9	2.49	3.93	1.57	0.48	3.03/3.03	96.3
	MRCI+Q	224.1151	2.294	58.5						/3.03	98

[a] Internally contracted MRCI. [b] +Q refers to the multireference Davidson correction. [c] $\langle\mu\rangle$ calculated as expectation value; μ_{FF} calculated by the finite field method. [d] Ref 13. [e] QCISD(T)/6-311+G(2df)/MP2(full)/6-311+G*. [f] State-averaged CASSCF.

(+Q) level. According to diagram 1, this rather weak bonding of the X $^2\Pi$ state is the result of a charge transfer from Mg to B via the σ frame and from B to Mg through the π frame, amounting to a total electron transfer to the B atom of about 0.2 e^- and a σ, $^1/_2$ π (one electron) bonding character.

The first excited state, $A^2\Sigma^+$ of MgB located 9.6 kcal/mol above the X state, as expected from diagram 2, is slightly or van der Waals bound by 2.28 (2.8) kcal/mol at the MRCI(+Q) level.

The next two states, $2^4\Sigma^-$ and $3^4\Pi$, are strictly degenerate within the accuracy of our calculations, located about 20.5 kcal/mol above the ground state and both correlating to Mg ($3s^13p^1$; ^3P) + B ($2s^22p^1$; ^2P). However, their electronic structure is quite different as evidenced from diagrams 3 and 4. The bonding in $^4\Sigma^-$ comprises one σ and two $^1/_2$ π bonds as compared to a $^1/_2$ σ and a $^1/_2$ π of the $3^4\Pi$ state. This is reflected in the equilibrium bond distance of $3^4\Pi$, which is 0.06 Å larger than the bond length of the $^4\Sigma^-$ state. Of course, both states have identical

TABLE 2: Leading CASSCF Configuration Functions and Mulliken Atomic Distributions of the First Four States of MgB Molecule

		Mg				B			
state	configurations[a]	3s	$3p_z$	$3p_x$	$3p_y$	2s	$2p_z$	$2p_x$	$2p_y$
$X^2\Pi$	$0.91/\sqrt{2}\lvert 1\sigma^2 2\sigma^2(1\pi_x^1 + i1\pi_y^1)\rangle$	1.37	0.20	0.08	0.08	1.77	0.54	0.46	0.46
$A^2\Sigma^{+b}$	$0.91\lvert 1\sigma^2 2\sigma^2 3\sigma^1\rangle$	1.62	0.23	0.04	0.04	1.83	1.06	0.06	0.06
$2^4\Sigma^-(1)$	$0.95\lvert 1\sigma^2 2\sigma^1 1\pi_x^1 1\pi_y^1\rangle$	0.99	0.16	0.21	0.21	1.55	0.25	0.77	0.77
$3^4\Pi(1)$	$0.97/\sqrt{2}\lvert 1\sigma^2 2\sigma^1 3\sigma^1(1\pi_x^1 + i1\pi_y^1)\rangle$	0.91	0.53	0.05	0.05	1.62	0.83	0.46	0.46

[a] Our orbital enumeration refers only to the five valence electrons, i.e., we do not count the doubly occupied four σ and two π "core" orbitals. [b] MRCI level.

TABLE 3: Absolute Energies *E* (hartree), Bond Lengths r_e (Å), Binding Energies D_e (kcal/mol) with Respect to the Adiabatic Atoms, Harmonic Frequencies and Anharmonic Corrections ω_e, $\omega_e x_e$ (cm^{-1}), Rotational Vibrational Couplings α_e (cm^{-1}), Centrifugal Distortions $\bar{D}_e$ (cm^{-1}), and Energy Separations T_e (kcal/mol) of the B_2 Molecule at CASSCF, MRCI,[a] and MRCI+Q[b]/cc-pVQZ Levels. Experimental and Previous Theoretical Results Are Also Included.

state	method	$-E$	r_e	D_e	ω_e	$\omega_e x_e$	α_e (10^{-2})	$\bar{D}_e$ (10^{-6})	T_e
$X^3\Sigma_g^-$	CASSCF	49.221045	1.6144	61.31	1017.9	8.73	1.40	6.27	0.0
	MRCI	49.304129	1.5984	65.39	1039.2	9.03	1.44	6.38	0.0
	MRCI+Q	49.30797	1.599	65.1					0.0
	MRCI/[5s4p3d2f1 g][c]		1.600	65.6	1041				0.0
	QCISD(T)/6-311G*[d]	49.28005		60.53					
	PMP4(4)/6-311G(2df)[d]	49.28946		64.81					
	SDCI/(8s6p3d2f)[e]	49.272178	1.602	47.27					
	CASSCF/cc-pV5Z[f]	49.221420	1.6141	61.4	1018.2	8.8	1.40		
	MRCI/cc-pV5Z[f]	49.306057	1.5973	65.8	1040.6	9.1	1.44		
	CCSD(T)/cc-pCV6Z[g]	49.306720	1.5919	64.77	1050.4				
	CCSD(T)/cc-pCV6Z[g,h]	49.409725	1.5855	65.53	1059.3				
	MRCI/cc-pCV5Z[g]	49.306238	1.5971	65.78	1040.7				
	MRCI+Q/cc-pCV5Z[g]	49.310144	1.5973	65.53	1038.8				
	MRCI/cc-pCV5Z[g,h]	49.403777	1.5902	67.12	1052.5				
	MRCI+Q/cc-pCV5Z[g,h]	49.411557	1.5905	66.69	1049.3				
	MR-AQCC/cc-pVQZ[i]		1.5986	65.63	1037				
	expt		1.590[j]	69.6[j]	1051.3[j]	9.35[j]	1.4[j]		
	expt		1.590[l]	68.49 ± 14[k]	1052.7[l]				
	expt		1.5838[m]		1060[m]				
$a^5\Sigma_u^-$	CASSCF	49.221663	1.5441	131.20	1217.5	7.08	1.15	5.72	−0.39
	MRCI	49.296874	1.5253	142.91	1255.1	7.22	1.16	5.79	4.55
	MRCI+Q	49.29990	1.525	143.4					5.07
	MRCI/[5s4p3d2f1 g][c]		1.526	145	1245				4.86
	MR-AQCC/cc-pVQZ[i]		1.5250	143.68	1255				5.02
$A^3\Pi_u$	CASSCF	49.198041	1.7778	45.62	782.0	7.46	1.30	5.95	14.44
	MRCI	49.287904	1.7545	55.09	808.2	7.44	1.31	6.03	10.18
	MRCI+Q	49.29289	1.754	55.7					9.46
	MRCI/[5s4p3d2f1 g][c]		1.756	55.5	807				10.07
	MR-AQCC/cc-pVQZ[i]		1.7546	55.83	806				9.80
	expt[n]		1.74405		817.997	7.458	1.32	5.73	
$b^1\Delta_g$	CASSCF	49.194893	1.6365	44.90	972.9	9.87	1.49	6.32	16.41
	MRCI	49.283319	1.6172	52.30	996.9	9.88	1.52	6.46	13.06
	MRCI+Q	49.28777	1.618	52.4					12.7
	MRCI/[5s4p3d2f1 g][c]		1.619	52.6	973				12.97
	MR-AQCC/cc-pVQZ[i]		1.6175	52.76	995				12.87
	expt[o]		1.616						
$c^1\Sigma_g^+{}_{(G)}$[p]	CASSCF	49.185623	1.6503	36.57	928.5	10.95	1.60	6.60	22.23
	MRCI	49.270498	1.6438	44.05	903.9	16.05	1.96	7.14	21.10
	MRCI+Q	49.27466	1.648	44.2					20.9
	MRCI/[5s4p3d2f1g][c]		1.653	44.6	868				20.95
	MR-AQCC/cc-pVQZ[i]		1.6545	44.75	829				20.89
	expt[q]		1.650						
$c^1\Sigma_g^+{}_{(L)}$[p]	CASSCF	49.185270	1.9216	36.35	618.5	7.03	1.13	5.97	22.45
	MRCI	49.262114	1.8716	38.79					26.36
	MRCI+Q	49.26645	1.8438	39.1					26.1

[a] Internally contracted MRCI. [b] +Q refers to the multireference Davidson correction. [c] Ref 16a. [d] Ref 16b. [e] Ref 16c. [f] Ref 16d. [g] Ref 16e. [h] All electrons are correlated. [i] Ref 16f. [j] Ref 15a, D_0 value. [k] Ref 15b; thermochemical data, D_0 value. [l] Ref 15c. [m] Ref 15d. [n] Ref 15e; high-resolution Fourier transform emission spectroscopy. [o] Ref 15f; emission, UV and visible spectra of B_2. [p] Global (G) and local (L) minima. [q] Ref 15g; emission spectroscopy.

dissociation energies $D_e = 52$ kcal/mol at the MRCI level with respect to the adiabatic fragments $Mg(^3P) + B(^2P)$; see Figure 1. With respect to the ground-state asymptotic fragments, either state is unbound by about 8.5 kcal/mol because of the significant $Mg(^3P \leftarrow {}^1S)$ excitation energy of 2.603 eV (MRCI).

B_2. Table 3 lists our results on the first five states of B_2 ($X^3\Sigma_g^-$, $a^5\Sigma_u^-$, $A^3\Pi_u$, $b^1\Delta_g$, and $c^1\Sigma_g^+$), while corresponding PECs are plotted in Figure 2. Table 4 shows leading CASSCF configurations and Mulliken populations for these states. On the basis of the main CASSCF CFs and Mulliken popula-

tions, the bonding is adequately represented by the vbL diagrams 5−9.

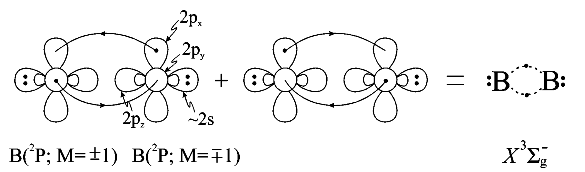

(5)

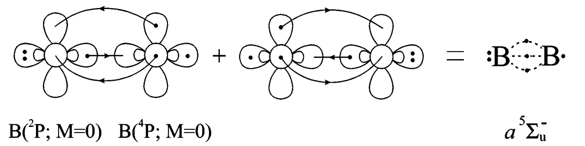

(6)

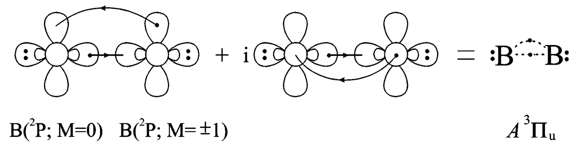

(7)

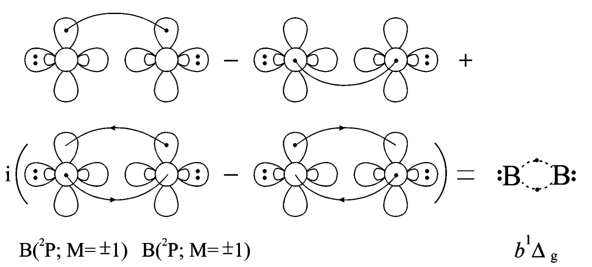

(8)

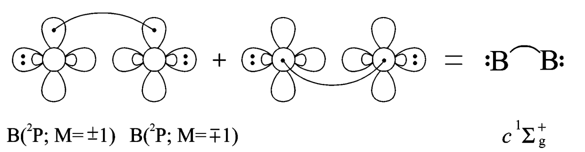

(9)

The really fascinating bonding structures of $X^3\Sigma_g^-$, $a^5\Sigma_u^-$, $A^3\Pi_u$, $b^1\Delta_g$, and $c^1\Sigma_g^+$ consist of two $^1/_2$ π, two $^1/_2$ π + $^1/_2$ σ, one $^1/_2$ σ + one $^1/_2$ π, one π (or two $^1/_2$ π), and one π bond, respectively. Our numerical results shown in Table 3 are in very good agreement with previous theoretical values as well as with relevant experimental findings (experimental results on the $a^5\Sigma_u^-$ state do not seem to exist). Observe that the first four excited states span an energy range of about 25 kcal/mol; they are practically evenly spaced, while in the $c^1\Sigma_g^+$ state, an avoided crossing around 3.5 bohr gives rise to a local minimum at 3.54 bohr. In addition, with the exception of the $a^5\Sigma_u^-$ state which correlates to the first excited state of a single boron atom, $B(^4P) + B(^2P)$, the remaining four states trace their lineage to the ground-state B atoms; see Figure 2.

B. The Triatomic MgB_2. Table 5 collects total energies, equilibrium geometries (r_{Mg-B}, r_{B-B}, $\angle BMgB \equiv \varphi$), atomization energies (AE) with respect to the adiabatic fragments Mg + 2B, dipole moments (μ), Mulliken charges (q_{Mg}, q_B), and energy separations (T_e) of 36 states/isomers at the CASSCF, MRCI, and MRCI+Q levels of theory; for the $^1A_1$ state only, MP2 and MP4 results are also reported. Figure 3 indicates relative energies of all MgB_2 states examined spanning an energy range of 4.2 eV; note that they are all bound with respect to the ground-state atoms $Mg(^1S) + 2B(^2P)$. In what follows, we describe in some detail the structure and bonding character of the first ten states in ascending energy order; the tenth state ($\tilde{g}^5A_2$) is located 32 kcal/mol above the $\tilde{X}^1A_1$ state.

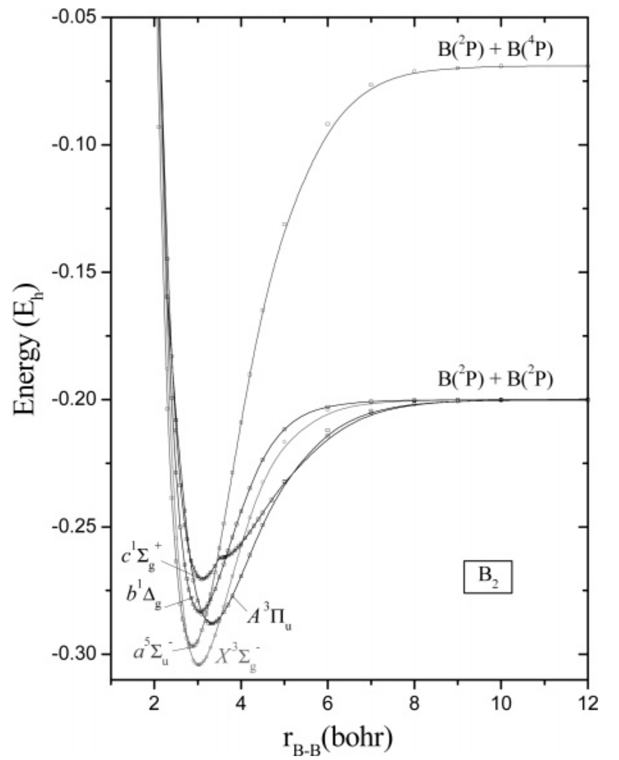

Figure 2. Potential energy curves of the first five states of the B_2 molecule at the MRCI/cc-pVQZ level of theory. All energies have been shifted by +49 E_h.

TABLE 4: Leading CASSCF Configuration Functions and Atomic Mulliken Distributions of the B_2 Molecule

state	configuration[a]	2s	$2p_z$	$2p_x$	$2p_y$
$X^3\Sigma_g^-$	$\|1\sigma_g^2[(0.89)1\sigma_u^2 - (0.33)2\sigma_g^2]1\pi_{ux}^1 1\pi_{uy}^1\rangle$	1.41	0.55	0.50	0.50
$a^5\Sigma_u^-$	$0.97\|1\sigma_g^2 1\sigma_u^1 2\sigma_g^1 1\pi_{ux}^1 1\pi_{uy}^1\rangle$	1.24	0.74	0.50	0.50
$A^3\Pi_u$	$0.92/\sqrt{2}\|1\sigma_g^2 1\sigma_u^2 2\sigma_g^1(1\pi_{ux}^1 + i1\pi_{uy}^1)\rangle$	1.63	0.77	0.29	0.29
$b^1\Delta_g$	$1/\sqrt{2}\{\|1\sigma_g^2[(0.87)1\sigma_u^2 - (0.35)2\sigma_g^2]1\pi_{ux}^1 1\bar{\pi}_{uy}^1\rangle + 0.62i\|1\sigma_g^2 1\sigma_u^2(1\pi_{ux}^2 - 1\pi_{uy}^2)\rangle\}$	1.39	0.57	0.50	0.50
$c^1\Sigma_{g\ (G)}^+$[b]	$0.61\|1\sigma_g^2 1\sigma_u^2(1\pi_{ux}^2 + 1\pi_{uy}^2)\rangle$	1.40	0.54	0.52	0.52
$c^1\Sigma_{g\ (L)}^+$[b]	$0.91\|1\sigma_g^2 1\sigma_u^2 2\sigma_g^2\rangle$	1.73	1.07	0.08	0.08

[a] Only the σ valence electrons are enumerated. [b] Global (G) and local (L) minimum.

$\tilde{X}^1A_1$ (BMgB). The main CASSCF equilibrium configurations of the $\tilde{X}^1A_1$ state, formally the ground state[18] (vide infra), and corresponding Mulliken atomic populations (Mg/B + B) are

$$|\tilde{X}^1A_1\rangle \approx |1a_1^2 2a_1^2 1b_1^2[(0.87)1b_2^2 - (0.26)3a_1^2]\rangle$$

$$3s^{0.96}3p_z^{0.08}3p_x^{0.23}3p_y^{0.13}/ (2s^{1.51}2p_z^{0.95}2p_y^{0.56})_{a_1}(2p_x^{1.69})_{b_1}(2s^{1.07}2p_y^{0.54}2p_z^{0.06})_{b_2}(2p_x^{0.08})_{a_2}$$

Note that only the eight valence electrons are counted. $(2s)_{a_1}$, $(2p_z)_{a_1}$, $(2p_x)_{b_1}$, and $(2p_y)_{b_2}$ refer to symmetric combinations and $(2p_y)_{a_1}$, $(2s)_{b_2}$, $(2p_z)_{b_2}$, and $(2p_x)_{a_2}$ to antisymmetric combinations of the relevant orbitals.

The formation of the BMgB $\tilde{X}^1A_1$ state can been thought of from either $B_2(X^3\Sigma_g^-/^3B_1$ in $C_{2v}) + Mg(^3P/^3B_1)$ or $MgB(^2\Pi$-(4)) + $B(^2P)$. Of course, the in situ Mg atom in the $^2\Pi(4)$ state of MgB is in its first excited $^3P(3s^13p^1)$ state; note that the $^2\Pi$-(4) state of MgB is not included in Table 1. Both channels are

TABLE 5: Absolute Energies E (hartree), Bond Lengths r(Å) and Angles ∠ BMgB≡φ (deg), Atomization Energies AE (kcal/mol) with Respect to the Adiabatic Products, Dipole Moments μ (debye), Mulliken Charges on Mg and B (central B for the MgBB geometries) Atoms q, and Energy Separations T_e (kcal/mol) of the MgB_2, at Different Levels of Theory.

geometry	state	method[a,b]	$-E$	r_{Mg-B}	r_{B-B}	φ	AE	$\langle\mu\rangle/\mu_{FF}$[c]	q_{Mg}	$-q_B$	T_e
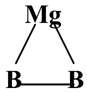	$\tilde{X}^1A_1$	CASSCF	248.91786	2.245	1.570	40.93	93.4	4.66/4.66	0.49	0.24	0.0
		MRCI	249.02006	2.225	1.560	41.06	108.1	5.00/4.99	0.52	0.26	0.0
		MRCI+Q	249.0259	2.225	1.561	41.1	109	/5.01			0.0
		MP2	248.98362	2.243	1.570	40.96	115.9				0.0
		MP4	249.02142	2.251	1.581	41.10	113.8				0.0
		RCCSD(T)	249.02159	2.223	1.560	41.08	107.9	/5.14			0.0
		RCCSD(T)[d]	249.02191	2.224	1.561	41.10	107.9	/5.11			0.0
		RCCSD(T)[e]		2.224	1.560	41.1					0.0
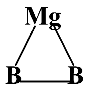	$\tilde{a}^3B_1$	CASSCF	248.91411	2.300	1.625	41.37	91.1	4.23/4.23	0.43	0.22	2.4
		MRCI	249.01880	2.279	1.617	41.55	107.3	4.71/4.75	0.46	0.23	0.79
		MRCI+Q	249.0254	2.279	1.617	41.5	109	/4.82			0.3
		RCCSD(T)	249.01976	2.272	1.616	41.67	106.7	/4.99			1.15
		RCCSD(T)[d]	249.01988	2.274	1.616	41.63	106.6	/4.98			1.27
		RCCSD(T)[e]		2.274	1.616	41.6					1.2
Mg−B−B	$\tilde{b}^3\Sigma^-$	CASSCF	248.90897	2.287	1.578		87.8	2.76/2.76	0.39	0.29	5.6
		MRCI	249.00285	2.266	1.578		97.3	3.02/3.12	0.41	0.33	10.8
		MRCI+Q	249.0085	2.265	1.581		98	/3.19			11
		RCCSD(T)[f]	249.00327	2.270	1.574		96.4	/2.88			11.5
		RCCSD(T)[d]	249.00298	2.268	1.573		96.0	/2.79			11.9
		RCCSD(T)[e]		2.263	1.556						11.9
Mg−B−B	$\tilde{c}^5\Sigma^-$	CASSCF	248.90938	2.291	1.564		149.2	2.24/2.24	0.39	0.29	5.3
		MRCI	249.00112	2.269	1.558		156.5	2.18/2.19	0.40	0.33	11.9
		MRCI+Q	249.0064	2.269	1.558		157	/2.18			12
		RCCSD(T)	249.00313	2.269	1.556		156.3	/2.16			11.6
		RCCSD(T)[d]	249.00339	2.269	1.556		156.3	/2.17			11.6
		RCCSD(T)[e]		2.270	1.556						11.8
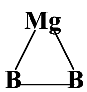	$\tilde{A}^1B_1$	CASSCF	248.89926	2.426	1.574	37.86	81.8	1.74/1.74	0.39	0.20	11.7
		MRCI	249.00001	2.355	1.575	39.07	95.5	2.37/2.88	0.40	0.20	12.6
		MRCI+Q	249.0062	2.335	1.580	39.5	97	/3.11			12
Mg−B−B	$\tilde{B}^1\boldsymbol{\Delta}$	CASSCF	248.87383	2.283	1.610		65.8	2.53/2.53	0.36	0.30	27.6
		MRCI	248.97827	2.257	1.607		81.9	3.11/3.27	0.38	0.33	26.2
		MRCI+Q	248.9855	2.256	1.610		84	/3.39			25
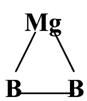	$\tilde{d}^3B_2$	CASSCF	248.87253	2.281	1.517	38.85	65.0	4.57/4.57	0.48	0.24	28.4
		MRCI	248.97416	2.254	1.503	38.94	79.3	5.05/5.11	0.50	0.25	28.8
		MRCI+Q	248.9802	2.251	1.504	39.0	80	/5.16			29
Mg−B−B	$\tilde{e}^3\Pi$	CASSCF	248.87170	2.132	1.517		64.5	7.38/7.38	0.53	0.38	29.0
		MRCI	248.97249	2.105	1.519		78.3	7.45/7.40	0.51	0.38	29.9
		MRCI+Q	248.9789	2.105	1.519		79	/7.32			29
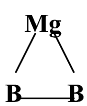	$\tilde{f}^3A_1$	CASSCF	248.87277	2.554	1.680	38.39	65.1	1.00/1.00	0.31	0.16	28.3
		MRCI	248.97071	2.535	1.672	38.51	77.2	1.30/1.38	0.34	0.17	31.0
		MRCI+Q	248.9770	2.538	1.675	38.5	78	/1.41			31
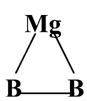	$\tilde{g}^5A_2$	CASSCF	248.87381	2.539	1.519	34.80	126.9	1.57/1.57	0.34	0.17	27.6
		MRCI	248.96958	2.511	1.504	34.86	136.7	1.68/1.67	0.36	0.18	31.7
		MRCI+Q	248.9751	2.512	1.504	34.9	137	/1.67			32
Mg−B−B	$10^3\Delta$	CASSCF	248.86512	2.269	1.591		60.3	1.78/1.78	0.38	0.32	33.1
		MRCI	248.96709	2.251	1.581		74.9	1.94/2.00	0.40	0.35	33.2
		MRCI+Q	248.9737	2.251	1.582		76	/2.03			33
Mg−B−B	$11^1\Sigma^+$	CASSCF	248.86554	2.279	1.618		60.6	2.56/2.56	0.35	0.29	32.8
		MRCI	248.96579	2.252	1.621		74.0	3.18/3.35	0.37	0.32	34.1
		MRCI+Q	248.9724	2.251	1.625		75	/3.49			34
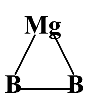	12^5B_1	CASSCF	248.86714	2.410	1.652	40.09	122.7	2.07/2.07	0.50	0.25	31.8
		MRCI	248.96575	2.401	1.644	40.03	134.3	2.09/2.09	0.48	0.24	34.1
		MRCI+Q	248.9719	2.404	1.643	40.0	135	/2.10			34
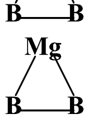	13^3A_2	CASSCF	248.86780	2.444	1.515	36.11	62.0	2.42/2.42	0.42	0.21	31.4
		MRCI	248.96462	2.413	1.504	36.31	73.3	2.66/2.81	0.42	0.21	34.8
		MRCI+Q	248.9702	2.413	1.504	36.3	74	/2.87			35
Mg−B−B	$14^1\Sigma^-$	CASSCF	248.85741	2.238	1.577		55.5	1.85/1.85	0.44	0.41	37.9
		MRCI	248.95868	2.241	1.574		69.6	1.87/1.92	0.42	0.40	38.5
		MRCI+Q	248.9653	2.244	1.576		71	/1.90			38
Mg−B−B	$15^1\Pi$	CASSCF	248.85659	2.183	1.528		55.0	4.93/4.93	0.57	0.46	38.5
		MRCI	248.95655	2.134	1.526		68.2	5.40/5.76	0.53	0.42	39.9
		MRCI+Q	248.9633	2.128	1.528		70	/5.87			39
Mg−B−B	$16^3\Sigma^+$	CASSCF	248.85625	2.263	1.599		54.8	1.71/1.71	0.37	0.32	38.7
		MRCI	248.95376	2.245	1.596		66.5	1.88/1.94	0.39	0.35	41.6
		MRCI+Q	248.9597	2.245	1.598		67	/1.97			42

TABLE 5: Continued.

geometry	state	method[a,b]	$-E$	r_{Mg-B}	r_{B-B}	φ	AE	$\langle\mu\rangle/\mu_{FF}$[c]	q_{Mg}	$-q_B$	T_e
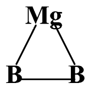	17^1A_2	CASSCF	248.82611	2.395	1.551	37.78	35.9	2.70/2.70	0.41	0.20	57.6
		MRCI	248.93301	2.362	1.588	39.29	53.5	3.02/3.15	0.38	0.19	54.6
		MRCI+Q	248.9404	2.357	1.596	39.6	55	/3.19			54
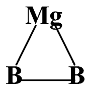	18^5B_2	CASSCF	248.83253	2.370	1.514	37.26	101.0	2.22/2.22	0.51	0.26	53.5
		MRCI	248.92674	2.366	1.504	37.08	109.8	2.24/2.24	0.50	0.25	58.6
		MRCI+Q	248.9321	2.369	1.503	37.0	110	/2.23			59
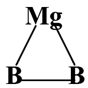	$19^1B_{2\ \mathrm{global}}$	CASSCF	248.82542	2.381	1.458	35.64	35.4	1.83/1.83	0.45	0.22	58.0
		MRCI	248.92670	2.366	1.450	35.68	49.5	1.80/1.81	0.41	0.21	58.6
		MRCI+Q	248.9329	2.366	1.450	35.7	51	/1.83			58
	$19^1B_{2\ \mathrm{local}}$	CASSCF	248.78913	2.449	2.381	58.16	12.7	3.01/3.01	0.42	0.21	80.8
		MRCI	248.89158	2.433	2.179	53.22	27.5	3.70/3.73	0.42	0.21	80.6
		MRCI+Q	248.8993	2.435	2.147	52.3	29	/3.74			79
Mg−B−B	$20^5\Pi$	CASSCF	248.81307	2.303	1.503		88.8	5.00/5.00	0.61	0.49	65.8
		MRCI	248.90048	2.299	1.501		93.3	4.77/4.76	0.58	0.49	75.0
		MRCI+Q	248.9056	2.302	1.502		93	/4.65			76
B−Mg−B	$21^1\Delta_g$	CASSCF	248.79209	2.317			14.5		0.53	0.27	78.9
		MRCI	248.90040	2.281			33.0		0.62	0.31	75.1
		MRCI+Q	248.9090	2.279			36				73
B−Mg−B	$22^3\Sigma_g^-$	CASSCF	248.79288	2.311			15.0		0.49	0.25	78.4
		MRCI	248.90011	2.274			32.9		0.59	0.30	75.3
		MRCI+Q	248.9085	2.273			35				74
B−Mg−B	$23^1\Sigma_g^+$	CASSCF	248.79112	2.320			13.9		0.54	0.27	79.5
		MRCI	248.89949	2.285			32.4		0.63	0.31	75.7
		MRCI+Q	248.9080	2.283			35				74
B−Mg−B	$24^1\Sigma_u^-$	CASSCF	248.79047	2.322			13.5		0.54	0.27	79.9
		MRCI	248.89888	2.287			32.1		0.64	0.32	76.0
		MRCI+Q	248.9074	2.286			35				74
B−Mg−B	$25^3\Pi_u$	CASSCF	248.78964	2.445			13.0		0.41	0.21	80.5
		MRCI	248.89687	2.394			30.8		0.50	0.25	77.3
		MRCI+Q	248.9055	2.391			33				76
B−Mg−B	$26^3\Delta_u$	CASSCF	248.78807	2.315			12.0		0.57	0.28	81.5
		MRCI	248.89662	2.282			30.7		0.65	0.33	77.5
		MRCI+Q	248.9052	2.281			33				76
B−Mg−B	$27^3\Sigma_u^+$	CASSCF	248.78748	2.318			11.6		0.57	0.29	81.8
		MRCI	248.89604	2.285			30.3		0.66	0.33	77.8
		MRCI+Q	248.9046	2.284			33				76
B−Mg−B	$28^5\Sigma_u^-$	CASSCF	248.78804	2.271			73.1		0.52	0.26	81.5
		MRCI	248.89446	2.245			89.6		0.62	0.31	78.8
		MRCI+Q	248.9027	2.245			93				77
B−Mg−B	$29^5\Delta_g$	CASSCF	248.78161	2.287			69.0		0.61	0.30	85.5
		MRCI	248.88957	2.260			86.5		0.69	0.35	81.9
		MRCI+Q	248.8980	2.259			89				80
B−Mg−B	$30^5\Sigma_g^+$	CASSCF	248.78110	2.288			68.7		0.61	0.31	85.8
		MRCI	248.88907	2.261			86.2		0.70	0.35	82.2
		MRCI+Q	248.8975	2.260			88				81
Mg−B−B	$31^5\Delta$	CASSCF	248.78881	2.275	1.798		73.6	−0.14/−0.14	0.21	0.17	81.0
		MRCI	248.88882	2.251	1.794		86.0	0.62/0.76	0.26	0.21	82.4
		MRCI+Q	248.8954	2.250	1.797		87	/0.87			82
Mg−B−B	$32^5\Sigma^+$	CASSCF	248.78620	2.276	1.801		71.9	−0.22/−0.22	0.20	0.16	82.6
		MRCI	248.88597	2.251	1.799		84.2	0.56/0.71	0.25	0.20	84.2
		MRCI+Q	248.8925	2.250	1.801		85	/0.82			84
B−Mg−B	$33^1\Pi_g$	CASSCF	248.76773	2.553			0.8		0.22	0.11	94.2
		MRCI	248.87498	2.446			17.1		0.37	0.19	91.0
		MRCI+Q	248.8841	2.434			20				89
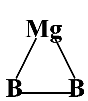	34^5A_1	CASSCF	248.77367	2.385	1.734	42.63	64.1	4.34/4.34	0.57	0.28	90.5
		MRCI	248.86926	2.303	1.696	43.21	73.7	5.01/5.32	0.59	0.29	94.6
		MRCI+Q	248.8754	2.297	1.692	43.22	74	/5.43			94
B−Mg−B	$35^5\Pi_g$	CASSCF	248.75807	2.224			54.3		0.55	0.28	100.3
		MRCI	248.86616	2.194			71.8		0.65	0.32	96.6
		MRCI+Q	248.8747	2.193			74				95

[a] Internally contracted MRCI. [b] +Q refers to the multireference Davidson correction. [c] $\langle\mu\rangle$ calculated as expectation value; μ_{FF} calculated by the finite field method. [d] RCCSD(T) based on CASSCF orbitals. [e] Ref 9, RCCSD(T)/aug-cc-pVQZ level of theory. [f] RCCSD(T) based on five configuration CASSCF orbitals.

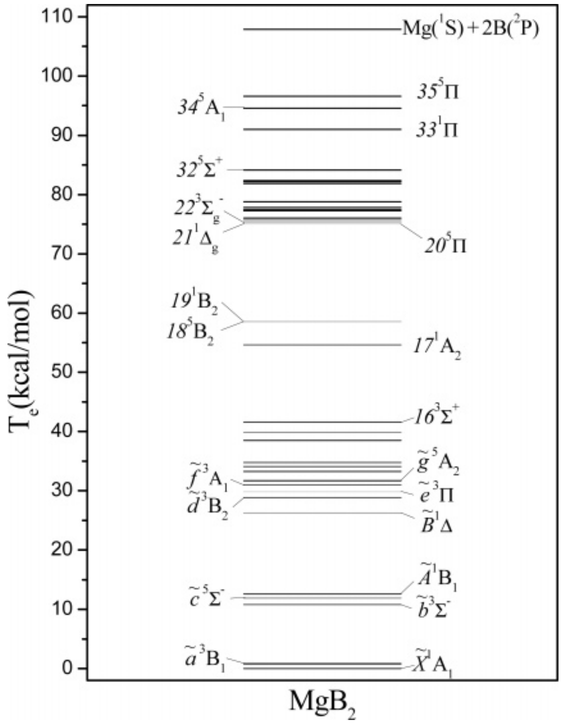

Figure 3. Relative energy levels of MgB_2 at the MRCI/cc-pVQZ level.

consistent with the following vbL bonding representation of the BMgB $\tilde{X}^1A_1$ ($={}^3B_1 \otimes {}^3B_1$) state.

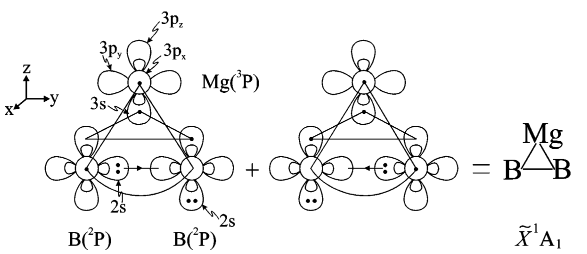

(10)

The bonding comprises one "σ"-like (in-plane) and one "π"-like (out-of-plane) $2e^-$−3 center bonds represented by the two isosceles triangles shown in diagram 10. The vbL diagram (10) is in accordance with the Mulliken distributions given above: About 0.7 e^- are transferred from the metal to the in situ B_2 moiety through the "π" plane, while about 0.2 e^- are moving back from B_2 to Mg through the "σ" plane. The BB bond length in the $\tilde{X}^1A_1$ state decreases considerably as compared to the free B_2 ($X^3\Sigma_g^-$) at the same level of theory, $\Delta r = -0.04$ Å (see Tables 3 and 5). Therefore, it is clear that the two B atoms can be considered bonded in the $\tilde{X}^1A_1$ state of MgB_2.

At infinity, the wave function can be described by the product $|^1S\rangle_{Mg} \times |^2P\rangle_B \times |^2P\rangle_B$ and the atomization energy with respect to the ground-state atoms (see Figure 4) is 108.1(109) kcal/mol at the MRCI(+Q) level of theory, Table 5. Correcting with respect to the zero-point harmonic vibrational (ZPE) energy, $\omega_1(B_2) = 453.6$, $\omega_2(A_1) = 494.7$, and $\omega_3(A_1) = 1079.6$ cm^{-1} as obtained at the MP2 level, the atomization energy becomes $108.1(109) - {}^1/_2(\omega_1 + \omega_2 + \omega_3) = 105.2(106)$ kcal/mol. With respect to the adiabatic products $B_2(b^1\Delta_g) + Mg(^1S)$ (see Figure 4 and diagram 8) the MRCI(+Q) dissociation energy is $D_e = 55.6(56)$ kcal/mol, or $D_0 = D_e - \text{ZPE(BMgB)} + \omega_e/2[B_2(b^1\Delta g)] = 55.6(56) - 2.90 + 1.42 = 54.1(55)$ kcal/mol.

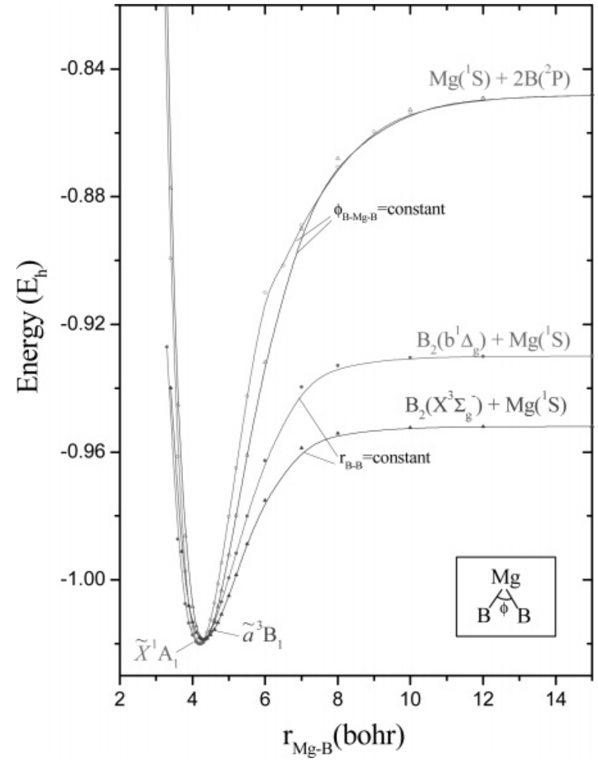

Figure 4. MRCI potential energy profiles of the $\tilde{X}^1A_1$ and $\tilde{a}^3B_1$ states of MgB_2 molecule, keeping the B−B distance or the angle φ at their equilibrium values. All energies have been shifted by $+248$ E_h.

Moving from C_{2v} [BMgB($\tilde{X}^1A_1$)] symmetry to the linear $D_{\infty h}$ structure, or $\tilde{X}^1A_1 \rightarrow {}^1\Delta_g$, the MRCI(+Q) barrier to linearity is 75.1(73) kcal/mol, Figure 5. The $^1\Delta_g$ state is the lowest of BMgB linear geometry giving rise to two Renner−Teller components, $\tilde{X}^1A_1$ and $\tilde{A}^1B_1$, upon bending. The bonding vbL diagram of the $^1\Delta_g$ structure is shown below.

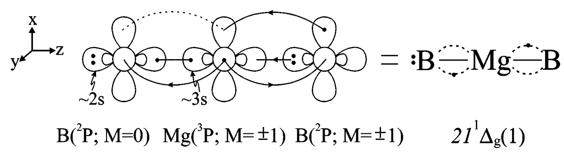

(11)

The CASSCF Mulliken atomic populations (Mg/B) $3s^{0.82}3p_z^{0.32}3p_x^{0.12}3p_y^{0.12}/2s^{1.67}2p_z^{0.68}\ 2p_x^{0.45}2p_y^{0.45}$ are in conformity with diagram 11. Table 5 lists numerical results concerning the $^1\Delta_g$ (transition) linear state.

$\tilde{a}^3B_1$ (BMgB). The leading equilibrium CASSCF configurations and atomic Mulliken populations of the $\tilde{a}^3B_1$ state, formally the first excited state of MgB_2[18] located 0.79(0.3)[1.15] kcal/mol above the $\tilde{X}^1A_1$ state at the MRCI(+Q)[CCSD(T)] level, are as follows (Mg/B+B):

$$|^3B_1\rangle = \sim|[0.89(1a_1^{\,2}2a_1^{\,2}3a_1^{\,1}) - 0.17(1a_1^{\,2}3a_1^{\,1}4a_1^{\,2})]1b_1^{\,1}1b_2^{\,2}\rangle$$

$$3s^{1.10}3p_z^{0.11}3p_x^{0.07}3p_y^{0.19}/(2s^{1.68}2p_z^{1.00}2p_y^{1.02})(2p_x^{0.86})(2s^{1.14}2p_y^{0.51}2p_z^{0.08})(2p_x^{0.05})$$

Figure 4 shows the potential energy profile with respect to Mg + B_2; the bond distance of B_2 is fixed to the equilibrium value of the $\tilde{a}^3B_1$ state along the potential curve but is relaxed to the

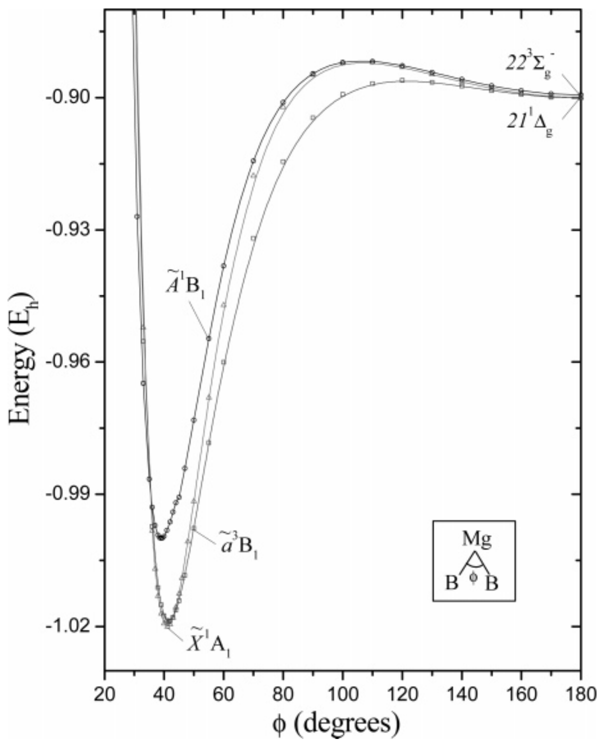

Figure 5. MRCI potential energy profiles of the $\tilde{X}^1A_1$, $\tilde{a}^3B_1$, and $\tilde{A}^1B_1$ states of MgB_2 with respect to the angle φ, while keeping the r_{Mg-B} distance at its equilibrium value. Energies shifted by +248 E_h.

$X^3\Sigma_g^-$ bond length at infinity. The bonding can be described by the vbL icon (12).

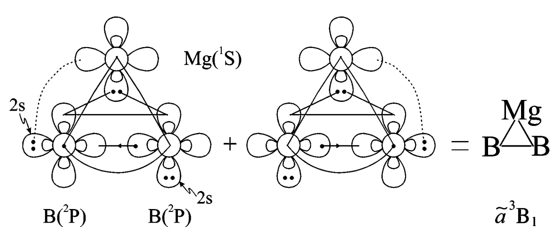

(12)

The in situ B_2 finds itself in the $A^3\Pi_u$ ($^3B_1$) state with the Mg in its ground ^1S state; however, as seen in Figure 4, it correlates to $B_2(X^3\Sigma_g^-)$ + Mg(^{1}S). The bonding is due to a transfer of about 0.7 e^- from the $3s^2(2a_1^2)$ pair of Mg to the empty $2p_z$ orbitals of B atoms ("in-plane", σ character), with a concomitant back transfer of 0.1 and 0.2 e^- from the $2p_x^1(b_1)$ single electron and $\sim 2s^2(b_2)$ pair of the B_2 moiety to the $3p_x$ and $3p_y$ empty orbitals of Mg, respectively; see diagram 12. Thus, a net charge of about 0.4 e^- is moving from Mg to B_2. With respect to $B_2(X^3\Sigma_g^-)$ + Mg(^{1}S), the MRCI(+Q) binding energy is 41.7(43) kcal/mol. The MRCI B−B bond distance and ∠BMgB angle increase by 0.06 Å and 0.5 deg as compared to the $\tilde{X}^1A_1$ state.

Figure 5 shows the potential energy profile of the $\tilde{a}^3B_1$ state with respect to the ∠BMgB angle. The corresponding linear structure BMgB of $^3\Sigma_g^-$ symmetry is (accidentally) degenerate to the $^1\Delta_g$ structure, which correlates to $\tilde{X}^1A_1$ (vide supra), with a barrier to linearity of 74.5 kcal/mol. The population analysis (Mg/B) $3s^{0.82}3p_z^{0.29}3p_x^{0.16}3p_y^{0.16}/2s^{1.68}2p_z^{0.68}2p_x^{0.44}2p_y^{0.44}$ supports the vbL icon (13).

$\tilde{b}^3\Sigma^-$ *(MgBB).* This is the second excited state of MgB_2 or the ground state of the linear MgBB isomer, located 11 kcal/mol above the (formal) ground state $\tilde{X}^1A_1$. The formation of

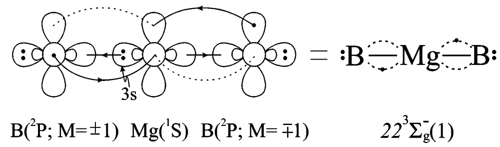

(13)

the molecule can be thought of as either MgB($X^2\Pi$) + B(^{2}P) or Mg(^{1}S) + $B_2(X^3\Sigma_g^-)$; the corresponding potential energy profiles are displayed in Figure 6. At the MRCI(+Q) level, the dissociation energies with respect to MgB + B or Mg + B_2 are 84.5(85) and 31.7(33) kcal/mol, respectively.

This is a truly multireference state as is evidenced from the leading CASSCF configurations

$$|\tilde{b}^3\Sigma^-\rangle \approx |[0.69(1\sigma^2 2\sigma^2 3\sigma^2) - 0.47(1\sigma^2 2\sigma^2 4\sigma^2)]1\pi_x^{\ 1}1\pi_y^{\ 1} + (1\sigma^2 2\sigma^2 3\sigma^1 4\sigma^1)[0.37(1\bar{\pi}_x^{\ 1}1\pi_y^{\ 1}) + 0.26(1\pi_x^{\ 1}1\bar{\pi}_y^{\ 1})]\rangle$$

With the help of the Mulliken CASSCF atomic populations

$$3s^{1.03}3p_z^{0.51}3p_x^{0.01}3p_y^{0.01}/2s^{1.33}2p_z^{0.93}2p_x^{0.49}2p_y^{0.49}/2s^{1.36}2p_z^{0.71}2p_x^{0.50}2p_y^{0.50}$$

the bonding can be captured by the vbL graph (14).

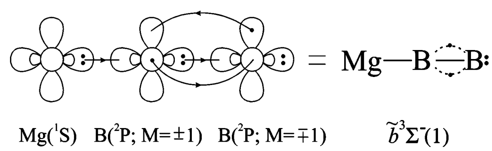

(14)

A total of 0.4 e^- are transferred from Mg to B_2 along the σ frame, about 0.3 e^- to the central B atom and 0.1 e^- to the second B directly linked to the central B atom.

The MRCI(+Q)[RCCSD(T)] atomization energy with respect to Mg(^{1}S) + 2B(^{2}P) is 97.3(98)[96.4] kcal/mol. Perhaps it should be mentioned at this point that the RCCSD(T) calculations were based on CASSCF orbitals. Finally, the bond distances r_{Mg-B} and r_{B-B} are shorter by 0.12 and 0.02 Å as compared to the free MgB($X^2\Pi$) and $B_2(X^3\Sigma_g^-)$, respectively.

$\tilde{c}^5\Sigma^-$ *(MgBB).* This linear high-spin excited state is located 12 kcal/mol above the $\tilde{X}^1A_1$ state and just 1 kcal/mol higher than the $\tilde{b}^3\Sigma^-$ state at the MRCI or MRCI+Q level. However, at the RCCSD(T) level of theory, the $\tilde{b}^3\Sigma^-$ and $\tilde{c}^5\Sigma^-$ states are degenerate; therefore, the labeling of the $^5\Sigma^-$ state as "c" is only formal. Similar results are reported in ref 8. As expected, this state has a single reference character, $|c^5\Sigma^-\rangle = \sim 0.96|1\sigma^2 2\sigma^2 3\sigma^1 4\sigma^1 1\pi_x^{\ 1}1\pi_y^{\ 1}\rangle$, which in conjunction with the Mulliken atomic populations (Mg/B/B)

$$3s^{1.01}3p_z^{0.54}3p_x^{0.01}3p_y^{0.01}/2s^{1.30}2p_z^{0.98}2p_x^{0.48}2p_y^{0.48}/2s^{1.32}2p_z^{0.72}2p_x^{0.51}2p_y^{0.51}$$

points to the following vbL bonding diagram:

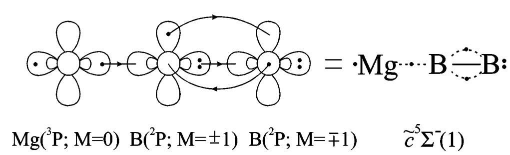

(15)

Note that, similarly to the $\tilde{b}^3\Sigma^-$ state, the in situ B_2 moiety is in the $^3\Sigma_g^-$ state, but the in situ Mg atom is excited to the $^3P(3s^1$-$3p^1)$ term. Nevertheless, by pulling apart the Mg atom, i.e., Mg + B_2, the $\tilde{c}^5\Sigma^-$ correlates to the first excited state of $B_2(a^5\Sigma^-)$ + Mg(^{1}S); see Figure 6. Imagining this state as formed from MgB + B, i.e., by pulling away the terminal B atom, the $\tilde{c}^5\Sigma^-$

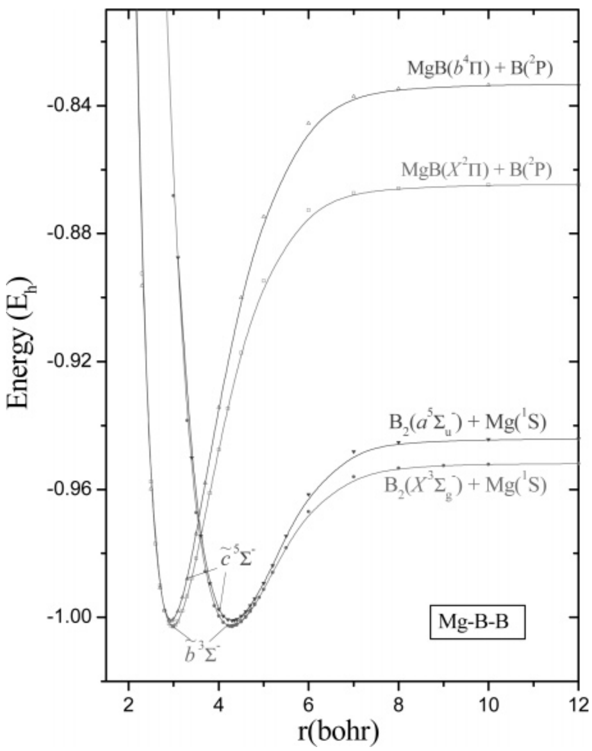

Figure 6. MRCI potential energy profiles of the $\tilde{b}^3\Sigma^-$ and $\tilde{c}^5\Sigma^-$ states of MgB_2 keeping the B−B or the Mg−B distances at their equilibrium values. Energies shifted by +248 E_h.

state correlates to the $b^4\Pi$ state of MgB (diagram 4) + B(^{2}P; M = ±1); see Figure 6.

With respect to the first channel, Mg(^{1}S) + B_2($a^5\Sigma^-$), the adiabatic binding energy is D_e = 35.2(37) kcal/mol; diabatically, namely, Mg(^{3}P) + B_2($X^3\Sigma^-$), D_e = 90.7(92) kcal/mol at the MRCI(+Q) level. With respect to the second channel, MgB-($b^4\Pi$) + B(^{2}P), D_e =103.3(104) kcal/mol.

$\tilde{A}^1B_1$ (BMgB). Formally, this is the fourth excited state and the third of C_{2v} symmetry, lying 12.6(12) kcal/mol higher than the $\tilde{X}^1A_1$ state. Its energy distance from the $\tilde{c}^5\Sigma^-$ is just 0.7 kcal/mol but by adding the Davidson correction these two states become degenerate; see Table 5 and Figure 3.

The most important CASSCF configurations and corresponding Mulliken atomic densities (Mg/B + B) are as follows:

$$|\tilde{A}^1B_1\rangle = \sim|1a_1^{\,2}2a_1^{\,2}3a_1^{\,1}[(0.88)1\bar{b}_1^{\,1}1b_2^{\,2} - (0.27)4a_1^{\,2}1\bar{b}_1^{\,1}]\rangle$$

$$3s^{1.03}3p_z^{0.40}3p_x^{0.03}3p_y^{0.07}/(2s^{1.59}2p_z^{1.43}2p_y^{0.58})(2p_x^{0.88})(2s^{1.14}2p_y^{0.51}2p_z^{0.10})(2p_x^{0.05})$$

As in the case of the $\tilde{X}^1A_1$, the wave function of the $\tilde{A}^1B_1$ state at infinity can be described by the product |Mg(^{1}S)⟩ × |B(^{2}P)⟩ × |B(^{2}P)⟩, but the in situ Mg atom is in its first excited state, ^{3}P($3s^13p^1$). The molecule can be thought of either as Mg-(^{3}P) + B_2($X^3\Sigma_g^-$) or as MgB + B(^{2}P). The bonding is graphically shown in diagram 16. A total of about 0.4 e^- are

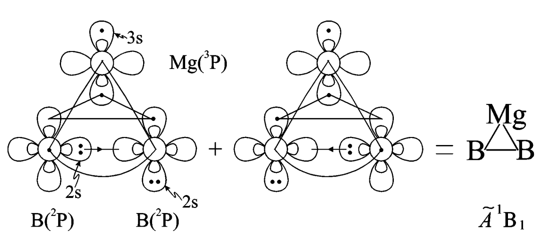

(16)

transferred from Mg to B_2: 0.6 e^- are moving from Mg to B through the $\sigma(a_1)$ plane (2 e^- − 3 centers), while about 0.2 e^- are back-transferred through the π (1 e^- − 3 centers) plane and $\sigma(b_2)$ bond.

The MRCI(+Q) atomization energy with respect to Mg(^{1}S) + 2B(^{2}P) is 95.5(97) kcal/mol. In comparison with the ground state, the Mg−B distance increases by 0.13 Å, while the B−B one increases only slightly.

$\tilde{B}^1\Delta$(MgBB), $\tilde{e}^3\Pi$(MgBB). The fifth and seventh excited states have linear geometry; they are of symmetries $^1\Delta$ and $^3\Pi$ and are located 26 and 30 kcal/mol above the ground state, respectively (Figure 3). Their leading CASSCF equilibrium configurations and atomic Mulliken population are (Mg/B/B)

$$|\tilde{B}^1\Delta_1\rangle = \sim|[0.56(1\sigma^22\sigma^23\sigma^2) - 0.35(1\sigma^22\sigma^24\sigma^2)](1\pi_x^{\,2} - 1\pi_y^{\,2})\rangle$$

$$3s^{1.13}3p_z^{0.42}3p_x^{0.02}3p_y^{0.02}/2s^{1.35}2p_z^{0.86}2p_x^{0.52}2p_y^{0.52}/2s^{1.37}2p_z^{0.73}2p_x^{0.46}2p_y^{0.46}$$

$$|\tilde{e}^3\Pi_1\rangle = \sim 1/\sqrt{2}|[0.90(1\sigma^22\sigma^23\sigma^1) - 0.19(1\sigma^23\sigma^14\sigma^2)](1\pi_x^{\,1}1\pi_y^{\,2} + 1\pi_x^{\,2}1\pi_y^{\,1})\rangle$$

$$3s^{1.11}3p_z^{0.07}3p_x^{0.07}3p_y^{0.16}/2s^{1.18}2p_z^{0.64}2p_x^{0.51}2p_y^{1.02}/2s^{1.24}2p_z^{0.67}2p_x^{0.41}2p_y^{0.78}$$

The bonding character of both states is captured by the vbL diagrams 17 and 18.

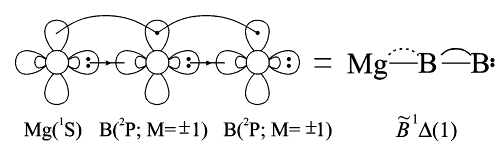

(17)

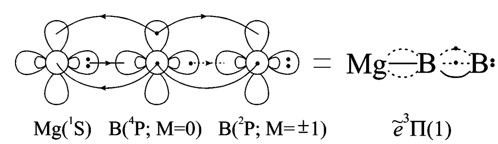

(18)

From diagram 17, it is obvious that in the $\tilde{B}^1\Delta$ state its "natural constituents" are Mg(^{1}S) + B_2($b^1\Delta_g$; Scheme 8). One π bond (B−B) and two σ bonds tie the molecule together, giving rise to an atomization energy of 81.9(84) kcal/mol at the MRCI-(+Q) level. Note that the B−B bond distance [1.607(1.610) Å] in the $\tilde{B}^1\Delta$ state is practically the same as the bond distance of the free B_2 in the $b^1\Delta_g$ state [1.617(1.618) Å], as the vbL diagram (17) suggests.

In the $\tilde{e}^3\Pi$ state, the central in situ B atom is in its first excited ^{4}P($2s^12p^2$) state; therefore, the in situ B_2 molecule is in the $^3\Pi_g$-(2) state (not included in Table 3). From vbL diagrams 17 and 18, it is suggested that the Mg−B and B−B bond lengths in the $\tilde{e}^3\Pi$ state should be shorter than the corresponding ones in the $\tilde{B}^1\Delta$ state. The Mg−B σ bond in the $\tilde{e}^3\Pi$ state should decrease, because the Mg(^{1}S) atom faces a more "exposed" B(^{4}P) atom, and this is indeed what is observed: The Mg−B and B−B bond lengths are shorter by 0.15 and 0.09 Å in the $\tilde{e}^3\Pi$ state as compared to the $\tilde{B}^1\Delta$ state. These differences are in agreement with the observed ones in the appropriate states of the free MgB [$^4\Sigma^-$(3), $X^2\Pi$] and B_2 [$^3\Pi_u$(2), $b^1\Delta_g$] molecules. Finally, the atomization energy of the $\tilde{e}^3\Pi$ state with respect to the ground-state atoms Mg(^{1}S) + 2B(^{2}P) (asymptotic products) is 78.3(79) kcal/mol.

$\tilde{d}^3B_2$(BMgB), $\tilde{f}\,^3A_1$(BMgB), and $\tilde{g}^5A_2$(BMgB). These are the last discussed states in the present work; they are of V-shaped geometry located 29, 31, and 32 kcal/mol above the $\tilde{X}^1A_1$ state (Table 5, Figure 3). Their leading equilibrium CASSCF CFs, Mulliken populations, and bonding vbL graphical representations follow:

$$|\tilde{d}^3B_2\rangle = \sim|[0.88(1a_1^2 2a_1^2 3a_1^1) + 0.22(1a_1^2 3a_1^1 4a_1^2)]1b_1^2 1b_2^1\rangle$$

$$3s^{1.02}3p_z^{0.11}3p_x^{0.24}3p_y^{0.05}/(2s^{1.68}2p_z^{0.92}2p_y^{1.09})(2p_x^{1.59})(2s^{0.64}2p_y^{0.34}2p_z^{0.05})(2p_x^{0.08})$$

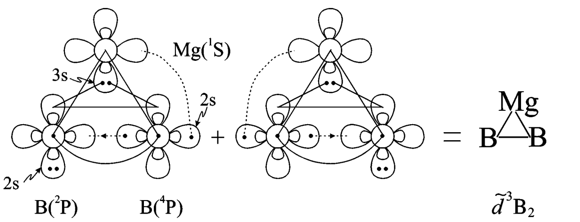

(19)

$$|\tilde{f}^3A_1\rangle = \sim 0.92|1a_1^2 2a_1^2 3a_1^1 4a_1^1 1b_2^2\rangle$$

$$3s^{1.10}3p_z^{0.45}3p_x^{0.00}3p_y^{0.08}/(2s^{1.73}2p_z^{1.35}2p_y^{1.16})(2p_x^{0.08})(2s^{1.27}2p_y^{0.46}2p_z^{0.10})(2p_x^{0.04})$$

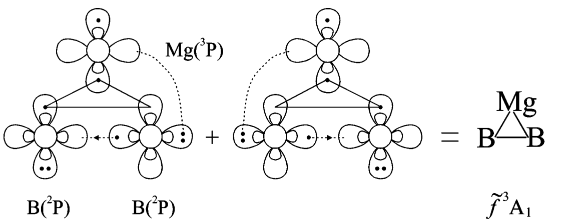

(20)

$$|\tilde{g}^5A_2\rangle = \sim 0.92|1a_1^2 2a_1^2 3a_1^1 4a_1^1 1b_1^1 1b_2^1\rangle$$

$$3s^{1.16}3p_z^{0.40}3p_x^{0.03}3p_y^{0.03}/(2s^{1.73}2p_z^{1.36}2p_y^{1.14})(2p_x^{0.92})(2s^{0.68}2p_y^{0.33}2p_z^{0.07})(2p_x^{0.03})$$

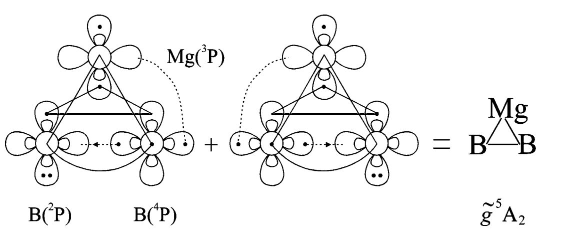

(21)

Diagrams 19 and 21 show that the two in situ B atoms are nonequivalent, one in the ground (^{2}P) and the other in its first excited ^{4}P state. But obviously, they should be equivalent on account of symmetry; the mirror images with respect to a symmetry plane bisecting the B$\hat{M}$gB angle ensure the C_{2v} symmetry invariance. Note also that, in the $\tilde{g}^5A_2$ state, two of the in situ atoms, the (unique) Mg and "one" of B atoms are excited.

Approximately 0.5, 0.3, and 0.3 e$^-$ are transferred from the Mg atom to the B_2 moiety in the $\tilde{d}^3B_2$, $\tilde{f}\,^3A_1$, and $\tilde{g}^5A_2$ states, respectively. It is interesting that the B−B distance in the $\tilde{d}^3B_2$ and $\tilde{g}^5A_2$ states is the smallest of all the MgB_2 states presently studied, about 0.1 Å shorter than the free $B_2(X^3\Sigma_g^-)$. Finally, the adiabatic MRCI(+Q) atomization energies with respect to Mg(^{1}S) + 2B(^{2}P)[$\tilde{d}^3B_2$, $\tilde{f}\,^3A_1$] and Mg(^{3}P) + 2B(^{2}P)[$\tilde{g}^5A_2$], are 79.3 (80), 77.2 (78), and 136.7 (137) kcal/mol, respectively.

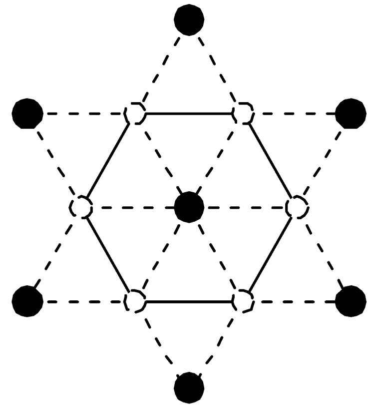

Figure 7. Projection of the crystal structure of MgB_2 looking from above and along the *c* axis (*P*/*mmm*), ●−● (Mg−Mg) = 3.08 Å, ○−○ (B−B) = 1.78 Å, ●−○(Mg−B) = 2.50 Å, ∠BMgB≡φ = 41.6°.

Numerical results for the remaining 24 states presently investigated are listed in Table 5, 6 of which are V-shaped, 8 linear of the MgBB type, and 10 linear of centrosymmetric configuration, B−Mg−B. Two of the centrosymmetric structures previously described, $^1\Delta_g$ and $^3\Sigma_g^-$, are transition states, but we did not try to calculate frequencies for the remaining 10 B−Mg−B states.

4. Summary and Remarks

Motivated by the recently discovered high superconducting transition temperature $T_c = 39$ K of crystalline MgB_2, we have examined by all-electron ab initio multireference and coupled-cluster methods the isolated MgB_2. A total of 36 states (including some transition states) were calculated spanning an energy range of 4.2 eV, all of which are bound with respect to the ground-state atoms, Mg(^{1}S) + 2B(^{2}P). In addition, we have calculated full potential energy curves for 17 states of the diatomic MgB. As far as we know, only 2 theoretical studies exist in the literature on MgB,[13,14] while experimental results are completely lacking.

Focusing on the triatomic MgB_2, our most import findings can be summarized as follows.

(a) Although formally the ground state is of $^1A_1$ symmetry, a strong contender is a $^3B_1$ state differing in energy by less than 1 kcal/mol, $T_e = 0.79(0.3)$ kcal/mol at the MRCI(+Q) level. In other words, the $^1A_1$ and $^3B_1$ states are degenerate within the accuracy of our calculations.

(b) In all states, about 0.2 to 0.6 electrons are moving from the Mg atom to the in situ B_2 moiety.

(c) The next V-shaped state ($\tilde{A}^1B_1$) is located 12 kcal/mol above the $\tilde{X}^1A_1$, while two more C_{2v} states ($\tilde{d}^3B_2$, $\tilde{f}\,^5A_2$) are well-separated from the ground state, located about 30 kcal/mol higher.

(d) The bonding in most of the MgB_2 states studied here, but in particular the V-shaped ones, is quite unconventional because of the extraordinary bonding agility of the B atom and the ensuing unusual distribution of the active electrons on the B_2 molecule.

(e) Schematically, the spatial arrangement of the atoms of crystalline MgB_2 (space group *P*6/*mmm*) is shown in the projection in Figure 7, looking down and along the (unique) *c* crystallographic axis. The top plane is formed of Mg (●) atoms, and the plane underneath of B atoms (○). The three atoms of the MgB_2 units are in special crystallographic positions, namely

(0, 0, 0), ($^1/_3$, $^2/_3$, $^1/_2$), and ($^2/_3$, $^1/_3$, $^1/_2$) corresponding to Mg, B, and B atoms, respectively (see also ref 3).

From Figure 7, we observe that the solid structure is composed of identical isosceles triangles; therefore, relevant states of a single (isolated) MgB_2 molecule (and excluding higher states) can only be the two practically degenerate $\tilde{X}^1A_1$ and $\tilde{a}^3B_1$ states.

Mg−B and B−B distances are larger in the crystal structure as compared to the isolated molecule by about 0.25 and 0.20 Å, respectively. Remarkably, however, the ∠BMgB ($=\varphi$) angle is identical in the solid state ($\varphi = 41.6°$) and in the $\tilde{X}^1A_1$($\varphi = 41.1°$) or $\tilde{a}^3B_1$($\varphi = 41.6°$) molecular state.

(f) Our calculations indicate that electrons are fed copiously from the Mg layers to the B layers. We dare suggest that in the crystalline environment each Mg atom can lose up to one electron or more, transferred to two equivalent B atoms. Our bonding analysis of the $\tilde{X}^1A_1$ and $\tilde{a}^3B_1$ states points to σ (in-plane) and π (out-of-plane) bands in the solid phase. In the latter, the superconductivity is allowed by both perpendicular (π bands) and parallel (σ bands) bands to the boron sheets.[2]

Obviously, the connection of an isolated species (here, MgB_2) to the relevant polymeric crystal (here, $(MgB_2)_x$) is far from trivial. We hope however that the present study and analysis can be of some help for the better understanding of this very interesting material.

Acknowledgment. D.T. expresses her gratitude to the Academy of Athens for financial support. Part of this work is supported by the Greek Ministry of Education and European Union through the E.P.E.A.K. program PYTHAGORAS (70/3/7373) for basic research.

References and Notes

(1) Nagamatsu, J.; Nakagawa, N.; Muranaka, T.; Zenitani, Y.; Akimitsu, J. *Nature (London)* **2001**, *410*, 63.

(2) See, for instance, the very interesting article by Canfield, P. C.; Crabtree, G. W. *Phys. Today* **2003**, *56* (3), 34 and references therein.

(3) Jones, M. E.; Marsh, R. E. *J. Am. Chem. Soc.* **1954**, *76*, 1434.

(4) See, for example, (a) Bugoslavsky, Y.; Perkins, G. K.; Qi, X.; Cohen, L. F.; Caplin, A. D. *Nature (London)* **2001**, *411*, 563. (b) Jim, S.; Mavoori, H.; Bower, C.; van Dover, R. B. *Nature (London)* **2001**, *410*, 563. (c) Kang, W. N.; Kim, H.-J.; Choi, E.-M.; Jung, C. U.; Lee, S.-I. *Science* **2001**, *292*, 1521.

(5) (a) An, J. M.; Pickett, W. E. *Phys. Rev. Lett.* **2001**, *86*, 4366. (b) Choi, H.-J.; Roundy, D.; Sun, H.; Cohen, M. L.; Louie, S. G. *Phys. Rev. B* **2002**, *66*, 20513. (c) Li, Z.; Yang, J.; Hou, L. G.; Zhu, Q. *Phys. Rev. B* **2002**, *65*, 100507. (d) Nakamura, J. et al. *Phys. Rev. B* **2003**, *68*, 64515. (e) Martin, I. I.; Anderson, O. K.; Jepsen, O.; Golubov, A. A.; Dolgov, O. V.; Kortus, J. *Phys. Rev. B* **2004**, *69*, 56501.

(6) V. Grignard received the Nobel Prize (1/2) in 1912, for the discovery of the so-called Grignard reagent which in recent years has greatly advanced the progress of organic chemistry. In 1976, the Nobel Prize in chemistry was given to W. N. Limpscomb, Jr., for his studies on the structure of boranes illuminating problems of chemical bonding. H. C. Brown was the recipient of the 1979 Nobel Prize (1/2) in chemistry for the development of the use of boron compounds into important reagents in organic synthesis. James, L. K. In *Nobel Laureates in Chemistry, 1901−1992* American Chemical Society and the Chemical Heritage Foundation: Washington, DC, 1993. Also, *List of the Nobel Prize Winners 1901−1993*; Nobel Committees for Physics and Chemistry; The Royal Swedish Academy of Sciences: Stockholm, Sweden, 1994.

(7) Ercoç, Ş. *Int. J. Mod. Phys. C* **2003**, *14*, 483.

(8) Yang, C.-L.; Zhang, X.; Han, K.-L. *THEOCHEM* **2004**, *677*, 11.

(9) Lee, E. P. F.; Wright, T. G. *J. Phys. Chem. A* **2004**, *108*, 7424.

(10) Dunning, T. H., Jr. *J. Chem. Phys.* **1989**, *90*, 1007.

(11) (a) Werner, H.-J.; Knowles, P. J. *J. Chem. Phys.* **1988**, *89*, 5803. (b) Knowles, P. J.; Werner, H.-J. *Chem. Phys. Lett.* **1988**, *145*, 514. (c) Werner, H.-J.; Reinsch, E. A. *J. Chem. Phys.* **1982**, *76*, 3144. (d) Werner, H.-J. *Adv. Chem. Phys.* **1987**, *69*, 1.

(12) MOLPRO 2000 is a package of ab initio programs written by Werner, H.-J.; Knowles, P. J.; with contributions by Amos, R. D.; Bernhardsson, A.; Berning, A.; Celani, P.; Cooper, D. L.; Deegan, M. J. O.; Dobbyn, A. J.; Eckert, F.; Hampel, C.; Hetzer, G.; Korona, T.; Lindh, R.; Lloyd, A. W.; McNikolas, S. J.; Manby, F. R.; Meyer, W.; Mura, M. E.; Nicklass, A.; Palmieri, P.; Pitzer, R.; Rauhut, G.; Schuetz, M.; Stoll, H.; Stone, A. J.; Tarroni, R.; Thorsteinsson, T. University of Cardiff Consultants, Ltd., 2004; http://www.molpro.net.

(13) Boldyrev, A. I.; Gonzales, N.; Simons, J. *J. Phys. Chem.* **1994**, *98*, 9931.

(14) Pelegrini, M.; Roberto-Neto, O.; Machado, F. B. C. *Int. J. Quantum Chem.* **2003**, *95*, 205.

(15) (a) Douglas, A. E.; Herzberg, G. *Can. J. Res.* **1940**, *18*, 165. Huber, K. P.; Herzberg, G. *Molecular spectra and molecular structure IV. Constants of diatomic molecules*; Van Nostrand: Princeton, 1979. (b) Chase, M. W., Jr.; Davies, C. A.; Downey, J. R., Jr.; Frurip, D. J.; McDonald, R. A.; Syverud, A. N. *J. Phys. Chem. Ref. Data* **1985**, *14*, Suppl. 1. (c) Bredohl, H.; Dubois, I.; Nzohabonayo, P. *J. Mol. Spectrosc.* **1982**, *93*, 281. (d) Bredohl, H.; Dubois, I.; Melen, R. *J. Mol. Spectrosc.* **1987**, *121*, 128. (e) Brazier, C. R.; Carrick, P. G. *J. Chem. Phys.* **1994**, *100*, 7928. (f) Brazier, C. R.; Carrick, P. G. *J. Chem. Phys.* **1992**, *96*, 8684. (g) DeRose, M. E.; Carrick, P. G.; Brazier, R. *J. Mol. Spectrosc.* **1995**, *174*, 379.

(16) (a) Langhoff, S. R.; Bauschlicher, C. W., Jr. *J. Chem. Phys.* **1991**, *95*, 5882. (b) Martin, J. M. L.; Francois, J. P.; Gijbels, R. *Chem. Phys. Lett.* **1992**, *189*, 529. (c) McLean, A. D.; Liu, B.; Chandler, G. S. *J. Chem. Phys.* **1992**, *97*, 8459. (d) Peterson, K. A.; Kendall, R. A.; Dunning, T. H., Jr. *J. Chem. Phys.* **1993**, *99*, 9790. (e) Peterson, K. A.; Wilson, A. K.; Woon, D. E.; Dunning, T. H., Jr. *Theor. Chem. Acc.* **1997**, *97*, 251. (f) Müller, T.; Dallos, M.; Lischka, H.; Dubrovay, Z.; Szalay, P. G. *Theor. Chem. Acc.* **2001**, *105*, 227.

(17) Moore, C. E. *Atomic Energy Levels*; NSRDS-NBS Circular No. 35; U.S. Government Printing Office: Washington, DC, 1971.

(18) Our preliminary calculations using the cc-pVDZ basis reverse the order of the two lowest states ($^3B_1$ instead of $^1A_1$), but with the cc-pVTZ or cc-pVQZ basis sets, the $^1A_1$ becomes the ground state at the MRCI or MRCI+Q level of theory. Quadratic CI calculations, QCISD(T)/cc-pVQZ, also predict that the ground state is of $^1A_1$ symmetry.